

Article

# Entropy Generation on MHD Blood Flow of Nanofluid Due to Peristaltic Waves

Mohammad Mehdi Rashidi <sup>1,2</sup>, Muhammad Mubashir Bhatti <sup>3</sup>, Munawwar Ali Abbas <sup>4</sup> and Mohamed El-Sayed Ali <sup>5,\*</sup>

<sup>1</sup> Shanghai Key Lab of Vehicle Aerodynamics and Vehicle Thermal Management Systems, Tongji University, Shanghai 201804, China; mm\_rashidi@yahoo.com

<sup>2</sup> ENN-Tongji Clean Energy Institute of Advanced Studies, Tongji University, Shanghai 200072, China

<sup>3</sup> Shanghai Institute of Applied Mathematics and Mechanics, Shanghai University, Shanghai 200072, China; mubashirme@yahoo.com

<sup>4</sup> Department of Mathematics, Shanghai University, Shanghai 200444, China; munawwar@shu.edu.cn

<sup>5</sup> Mechanical Engineering Department, College of Engineering, King Saud University, P. O. Box 800, Riyadh 11421, Saudi Arabia

\* Correspondence: mali@ksu.edu.sa; Tel.: +966-114-676-672; Fax: +966-114-676-652

Academic Editors: Giulio Lorenzini and Omid Mahian

Received: 19 January 2016; Accepted: 24 March 2016; Published: 1 April 2016

**Abstract:** This present study describes the entropy generation on magnetohydrodynamic (MHD) blood flow of a nanofluid induced by peristaltic waves. The governing equation of continuity, equation of motion, nano-particle and entropy equations are solved by neglecting the inertial forces and taking long wavelength approximation. The resulting highly non-linear coupled partial differential equation has been solved analytically with the help of perturbation method. Mathematical and graphical results of all the physical parameters for velocity, concentration, temperature, and entropy are also presented. Numerical computation has been used to evaluate the expression for the pressure rise and friction forces. Currently, magnetohydrodynamics is applicable in pumping the fluids for pulsating and non-pulsating continuous flows in different microchannel designs and it also very helpful to control the flow.

**Keywords:** nanofluid; entropy; blood flow; magnetohydrodynamics

## 1. Introduction

Nanotechnology is the most important driving force for the major thermal engineering, biology, and industrial applications. In 1995, Choi [1] introduced the term that dilutes suspension of ultrafine particles in common liquids, named as nanofluids. Nanofluids can improve the thermal conductivity of the mixture. Nanofluid dynamics also find diverse applications in medical science and energetic. Basically, it is a fluid which is synthesized by dispersing the nano-particle in the base fluid, such as biofluids, oil, lubricants, and water. More examples include various types of heat exchangers [2,3], microchannel [4–6] and car radiators [7,8]. Another important mechanism of fluid transport which can be achieved through the progressive wave of contraction or expansion which spreads along the length of a distensible tube or channel containing different types of fluid is known as peristaltic flow. The movement of chyme in the gastrointestinal routs, swallowing food through the esophagus, and the movement of the ovum in the female fallopian tube are prominent examples of peristaltic flow. Peristaltic flow can also be found in industrial applications, such as in pumping for the transport of corrosive and sterile fluids. Due to these important applications, peristaltic flow has been the subject of intensive studies in both theoretical and experimental domains alike [9–13].

The main objectives of peristaltic motion are to investigate the secondary fluid motion as a possible fluid mixing mechanism and fluid motion within the pump. Moreover, peristaltic motion in

physiological sciences has opened a new dimension for researchers to manipulate their equipment for attaining better output in their respective field of interest. One of the most important fields in these areas is peristaltic blood flow. In fact, the basic idea of peristalsis in blood circulation was given by Nicoll [14] by explaining that the minute vessels of most vascular systems retain the power of contraction and expansion. Although, at that time he could not assign the word peristalsis, but this approach inspired the researchers to investigate experimentally, as well as theoretically. The rate at which kidney cells execute the regulation of the volume of water or salts in the body is affected by using drugs; similarly, the rate at which blood flows through arteries may also be affected or slowed down by the drugs. It is important to note that there is a significant difference between restoration and reparation. By using drugs, the damaged structures or function of a human body can be repaired only but restoration is not possible. Many researchers have studied various aspects of blood flow in normal diseases arteries and blood flow in arteries having a single stenosis. Blair [15] used the available experimental results on human blood and verified by plotting the square root of the strain-rate against the square root of the shear stress that the linearity with a non-zero value for the intercept on the stress axis. Blood flow through an arterial segment having multiple stenosis was investigated by Misra *et al.* [16]. He derived volumetric flow rate and pressure distribution and concluded that the wall shear stress and pressure drops are at a maximum at the throat of each stenosis and a minimum at the ends of each stenosis. Another important development in the history of bio-fluids is the investigation of nanoparticle separation technology which can be used to isolate a wide range of nanoparticles out of plasma with a minimum amount of manipulation [17]. This latest discovery enables researchers to study the mathematical modeling of drug delivery nanoparticle systems in blood flow. Table 1 shows the composition of blood and main features in a healthy human body. Some more investigations dealing with blood flow modeling can be viewed in the available references [18–21].

**Table 1.** Composition of blood and main features in a healthy adult male [22].

Plasma/Living Cells	Range
Erythrocytes	$4.5\text{--}5.2 \times 10^6 / \text{mm}^3$
Protids	70–80 g/L
Leukocytes	$4\text{--}10 \times 10^3 / \text{mm}^3$
Ions	295–310 mEq/L
Eosinophils	1%–2%
Lipids	5–7 g/L
Lymphocytes	20%–40%
Glucids	0.8–1.1 g/L
Neutrophils	40%–70%
Osmotic pressure	280–300 mOsm
Basophils	0.5%–1%
pH	7.39–7.41
Monocytes	2%–10%
Hematocrit	41%–47%
Platelets	$2\text{--}4 \times 10^5 / \text{mm}^3$

The presence of a magnetic field in the study of peristaltic flow is of great interest with regards to certain problems of physiological fluids such as blood, blood pump machines. Abbas *et al.* [22] solved a fundamental problem of magnetohydrodynamic (MHD) peristaltic blood flow of nanofluids in a non-uniform channel. This was the motivation towards estimating blood flow in arteries during electromagnetic hyperthermia. Computational study on LDL transfer from blood flow to the wall tissues of arteries has been studied by Wade and Karino [23]. Agrawal and Anwaruddin [24] studied a mathematical model of MHD peristaltic blood flow through a channel with flexible walls. They observed that the effect of a magnetic field can be utilized as a blood pump in carrying out cardiac operations. Sud *et al.* [25] explored the effect of a moving magnetic field on blood flow. Further, Abbasi *et al.* [26] developed a mathematical model of peristaltic transport of MHD fluid by considering

variable viscosity. Some relevant studies to magnetic field models can be found from the list of references [27–30].

During the past few years, the analysis of various physiological systems has been reported by various scientist. However, physiological systems are quite difficult and complicated even though they depict a certain amount of linearity. They also show unpredictable and chaotic behavior. Furthermore, in such types of systems, the analysis of heat and mass transfer involves great interest which arises due to its complex combination of stochastic and deterministic physiological processes. Another such type of system in human blood is oscillation. While a human body performs its normal daily routine, ambulatory blood pressure is a clinical procedure to analyze the blood pressure for every 20 to 30 min during 24 to 48 h. Blood flow enhances when a person performs different physical activities and in such types of situations, blood circulation remains unstable. When the environmental temperature rises up to 20 °C, then heat transfer takes place from the skin through the process of evaporation, and when the temperature falls below 20 °C then human body loses heat through conduction and radiation processes. In such types of cases, entropy plays an important role to scrutinize such systems. Entropy generation comprises of two main parts; (i) frictional factors, and (ii) thermal irreversibility. Bejan [31,32] originally formulated the analysis of entropy generation and found various applications, such as two-phase flows [33], MHD pumps, and electric generators [34]. More studies on entropy generation are available in references [35,36]. However, in none of the studies mentioned above are the peristaltic flow problems with entropy generation. There are very few attempts in which the entropy generation of the peristaltic flow of nanofluids is taken into account in the presence of a magnetic field. In fact, the presence of magnetic fields introduces additional dissipation that must be considered to supply the necessary input power to perform the required task. This can be acquired by minimizing entropy generation in the processes. It is necessary to minimize the entropy generation in energy optimization problems. Moreover, to assess the intrinsic irreversibilities in microfluidics and to investigate optimized operation conditions, entropy generation appears as a convenient tool.

With the above analysis in mind, the aim of the present investigation is to study the MHD peristaltic blood flow of nanofluid with entropy generation through a porous medium. The governing flow problem is modeled by taking the approximation of the long wavelength and creeping flow regime. The solution for the resulting non-linear partial differential equations is solved with the help of the homotopy perturbation method (HPM). The impact of various pertinent parameters for pressure rise, friction force, temperature profile, concentration profile, and entropy are plotted and discussed in detail.

## 2. Mathematical Formulation

Let us suppose the unsteady irrotational, hydromagnetic flow of a non-Newtonian Williamson fluid, being incompressible and electrically-conducting by an external magnetic field, applied through a two-dimensional non-uniform porous channel having a sinusoidal wave moving down towards its walls. We have selected a Cartesian coordinate system for the channel in such a way that  $\tilde{x}$  – axis is taken along the axial direction and  $\tilde{y}$  – axis is taken along the transverse direction as shown in Figure 1. The geometry of the governing flow problem can be described as:

$$H(\tilde{x}, \tilde{t}) = b(\tilde{x}) + \tilde{a} \sin \frac{2\pi}{\lambda} (\tilde{x} - \tilde{c}\tilde{t}), \quad (1)$$

where:

$$b(\tilde{x}) = b_0 + \tilde{x},$$

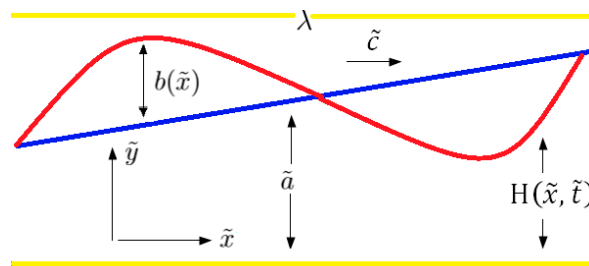


Figure 1. Geometry of the problem.

The governing equation of motion, continuity, thermal energy, and the nano-particle fraction for the peristaltic nanofluid of blood can be written as [22]:

$$\frac{\partial \tilde{u}}{\partial \tilde{x}} + \frac{\partial \tilde{v}}{\partial \tilde{y}} = 0, \tag{2}$$

$$\rho_f \left( \frac{\partial \tilde{u}}{\partial \tilde{t}} + \tilde{u} \frac{\partial \tilde{u}}{\partial \tilde{x}} + \tilde{v} \frac{\partial \tilde{u}}{\partial \tilde{y}} \right) = -\frac{\partial \tilde{p}}{\partial \tilde{x}} + \frac{\partial}{\partial \tilde{x}} S_{\tilde{x}\tilde{x}} + \frac{\partial}{\partial \tilde{y}} S_{\tilde{x}\tilde{y}} - \sigma_f B_0^2 \tilde{u} - \frac{\mu_f}{k} \tilde{u} + g \left[ (1-F) \rho_{f_0} \zeta (T - T_0) - (\rho_p - \rho_{f_0}) (F - F_0) \right], \tag{3}$$

$$\rho_f \left( \frac{\partial \tilde{v}}{\partial \tilde{t}} + \tilde{v} \frac{\partial \tilde{u}}{\partial \tilde{x}} + \tilde{v} \frac{\partial \tilde{v}}{\partial \tilde{y}} \right) = -\frac{\partial \tilde{p}}{\partial \tilde{y}} + \frac{\partial}{\partial \tilde{x}} S_{\tilde{y}\tilde{x}} + \frac{\partial}{\partial \tilde{y}} S_{\tilde{y}\tilde{y}} - \sigma_f B_0^2 \tilde{v} - \frac{\mu_f}{k} \tilde{v} + g \left[ (1-F) \rho_{f_0} \zeta (T - T_0) - (\rho_p - \rho_{f_0}) (F - F_0) \right], \tag{4}$$

$$(\rho c)_f \left( \frac{\partial T}{\partial \tilde{t}} + \tilde{u} \frac{\partial T}{\partial \tilde{x}} + \tilde{v} \frac{\partial T}{\partial \tilde{y}} \right) = \kappa \left( \frac{\partial^2 T}{\partial \tilde{x}^2} + \frac{\partial^2 T}{\partial \tilde{y}^2} \right) + (\rho c)_p D_B \left( \frac{\partial T}{\partial \tilde{x}} \frac{\partial F}{\partial \tilde{x}} + \frac{\partial F}{\partial \tilde{y}} \frac{\partial T}{\partial \tilde{y}} \right) + \frac{D_T}{T_0} \left( \left( \frac{\partial T}{\partial \tilde{x}} \right)^2 + \left( \frac{\partial T}{\partial \tilde{y}} \right)^2 \right) - \frac{\partial q_r}{\partial \tilde{y}} + Q_0, \tag{5}$$

$$\left( \frac{\partial F}{\partial \tilde{t}} + \tilde{u} \frac{\partial F}{\partial \tilde{x}} + \tilde{v} \frac{\partial F}{\partial \tilde{y}} \right) = D_B \left( \frac{\partial^2 F}{\partial \tilde{x}^2} + \frac{\partial^2 F}{\partial \tilde{y}^2} \right) + \frac{D_T}{T_0} \left( \frac{\partial^2 T}{\partial \tilde{x}^2} + \frac{\partial^2 T}{\partial \tilde{y}^2} \right) - k_1 (F - F_0). \tag{6}$$

Under the approximation of Rosseland for radiation, the radiative heat flux  $q_r$  is defined as:

$$q_r = -\frac{4\bar{\sigma}}{3K} \frac{\partial T^4}{\partial \tilde{y}}. \tag{7}$$

Let us consider that temperature within the nano-particle blood flow is very small, such that the term " $T^4$ " can be expanded about a free stream temperature " $T_0$ " as:

$$T^4 = T_0^4 + 4T_0^3 (T - T_0) + 6T_0^2 (T - T_0)^2 + \dots, \tag{8}$$

After neglecting the higher order terms in the above equation it can be written as:

$$T^4 \cong 4T_0^3 (T - T_0), \tag{9}$$

Using Equations (7)–(9) we get:

$$q_r = -\frac{16\sigma}{3K} \frac{\partial T}{\partial \tilde{y}}. \tag{10}$$

The extra stress tensor for Williamson fluid are defined as:

$$S = [\mu_\infty + (\mu_0 + \mu_\infty) (1 - \bar{\Gamma}\dot{\gamma})^{-1}] A_1, \tag{11}$$

where:

$$\dot{\gamma} = \sqrt{\frac{\text{trac}(A_1^2)}{2}}, \quad A_1 = (\text{grad } V + (\text{grad } V)^T).$$

In the above equation we have considered  $\mu_\infty = 0$  and  $\bar{\Gamma}\dot{\gamma} < 1$ . Now, it is convenient to define the non-dimensional quantities:

$$\begin{aligned}
 x &= \frac{\tilde{x}}{\lambda}, y = \frac{\tilde{y}}{b_0}, t = \frac{\tilde{t}}{\lambda}, u = \frac{\tilde{u}}{\tilde{c}}, v = \frac{\tilde{v}}{\tilde{c}\delta}, p = \frac{\tilde{p}b_0^2}{\lambda\mu\tilde{c}}, h = \frac{H}{b_0}, \phi = \frac{\tilde{a}}{b_0}, \text{Re} = \frac{\tilde{c}\rho\tilde{a}}{\mu}, \delta = \frac{\tilde{a}}{\lambda}, k \\
 &= \frac{\bar{k}}{\mu_f}, M = \sqrt{\frac{B^2\tilde{a}^2\sigma_f}{\mu_f}}, v = \frac{\tilde{v}\tilde{a}\tilde{c}}{\lambda}, \theta = \frac{T - T_0}{T_1 - T_0}, \Phi = \frac{F - F_0}{F_1 - F_0}, G_{rF} \\
 &= \frac{gb_0^3(\rho_p - \rho_{f_0})(F_1 - F_0)}{\rho_{f_0}v^2}, N_b = \frac{(\rho c)_p D_B(F_1 - F_0)}{\kappa}, \gamma = \frac{k_1 b_0^2}{v}, R_n \\
 &= \frac{16\sigma T_0^3}{3K\mu c_f}, \beta = \frac{Q_0 b_0^2}{(T_1 - T_0)v c_p}, N_t = \frac{(\rho c)_p D_T(T_1 - T_0)}{\kappa T_0}, \text{Pr} \\
 &= \frac{v(\rho c)_f}{\kappa}, G_{rT} = \frac{\zeta g b_0^3(T_1 - T_0)(1 - F_0)}{\rho_{f_0}v^2}, We = \frac{\Gamma\tilde{c}}{b_0}, \dot{\gamma} = \frac{\dot{\gamma}b_0}{\tilde{c}}.
 \end{aligned} \tag{12}$$

Let us consider the creeping flow under the assumptions of the long wavelength and low Reynolds number approximations. Using Equation (12) in Equations (2)–(6) we get the resulting equations in simplified form as:

$$\frac{\partial^2 u}{\partial y^2} + We \frac{\partial}{\partial y} \left( \frac{\partial u}{\partial y} \right)^2 - M^2 u - \frac{1}{k} u + G_{rT} \theta - G_{rF} \Phi - \frac{\partial p}{\partial x} = 0, \tag{13}$$

$$\left( \frac{1 + R_n \text{Pr}}{\text{Pr}} \right) \frac{\partial^2 \theta}{\partial y^2} + N_b \frac{\partial \theta}{\partial y} \frac{\partial \Phi}{\partial y} + N_t \left( \frac{\partial \theta}{\partial y} \right)^2 + \beta = 0, \tag{14}$$

$$\frac{\partial^2 \Phi}{\partial y^2} + \frac{N_t}{N_b} \left( \frac{\partial^2 \theta}{\partial y^2} \right) - \gamma \Phi = 0. \tag{15}$$

Subject to the respective boundary conditions:

$$\frac{\partial u(0)}{\partial y} = 0, \theta(0) = 0, \Phi(0) = 0, \tag{16}$$

$$u(h) = 0, \theta(h) = 1, \Phi(h) = 1, \tag{17}$$

where  $h = 1 + \frac{\lambda \bar{K} x}{b_0} + \phi \sin 2\pi(x - t)$ .

### 3. Entropy Generation Analysis

Entropy generation is derived from the energy and entropy balance for the case of heat and mass transfer. In the presence of a magnetic field it can be written as [36–38]:

$$\begin{aligned}
 S_{\text{gen}} &= \frac{\mathcal{K}_{nf}}{T_0^2} \left[ (\nabla T)^2 + \frac{16\sigma T^3}{3K} (\nabla T)^2 \right] + \frac{\mu_{nf}}{T_0} \left[ \left( \frac{\partial \tilde{u}}{\partial \tilde{y}} \right) + \bar{\Gamma} \dot{\gamma} \left( \frac{\partial \tilde{u}}{\partial \tilde{y}} \right)^2 \right] \left( \frac{\partial \tilde{u}}{\partial \tilde{y}} \right) + \frac{\sigma_{nf} B_0^2}{T_0} \tilde{u}^2 \\
 &+ \frac{\mu_{nf}}{k T_0} \tilde{u}^2 + \frac{RD_B}{F_0} (\nabla F)^2 + \frac{RD_B}{T_0} (\nabla F \cdot \nabla T).
 \end{aligned} \tag{18}$$

A characteristic entropy generation is given by as:

$$S_g = \frac{\mathcal{K}_f (T_1 - T_0)^2}{T_0^2 \tilde{b}_0^2}. \tag{19}$$

Using Equations (12) and (18), the dimensionless entropy generation number can be expressed as follows:

$$\begin{aligned}
 N_s = \frac{S_{gen}}{S_g} = & \left( \frac{\mathcal{K}_{nf}}{\mathcal{K}_f} \right) \left[ (1 + R_n) \left( \frac{\partial \theta}{\partial y} \right)^2 \right] + B_r \frac{1}{\Omega} \left( \frac{\mu_{nf}}{\mu_f} \right) \left[ \left( \frac{\partial \tilde{u}}{\partial \tilde{y}} \right) + We \left( \frac{\partial \tilde{u}}{\partial \tilde{y}} \right)^2 \right] \left( \frac{\partial \tilde{u}}{\partial \tilde{y}} \right) \\
 & + B_r \frac{1}{k\Omega} \left( \frac{\mu_{nf}}{\mu_f} \right) u^2 + M^2 B_r \frac{1}{\Omega} \left( \frac{\sigma_{nf}}{\sigma_f} \right) u^2 + \Gamma \left( \frac{\Lambda}{\Omega} \right)^2 \left( \frac{\partial \Phi}{\partial y} \right)^2 \\
 & + \zeta \left( \frac{\partial \theta}{\partial y} \right) \left( \frac{\partial \Phi}{\partial y} \right),
 \end{aligned} \tag{20}$$

where  $B_r, \Omega, \Lambda, \zeta, \Gamma$  are the Brinkman number, dimensionless temperature difference, concentration difference, constant parameter, and diffusive coefficient, which are represented as:

$$B_r = \frac{\tilde{c}^2 \mu_f}{\mathcal{K}_f (T_1 - T_0)}, \zeta = \frac{RD_B T_0}{\mathcal{K}_f} \left( \frac{F_1 - F_0}{T_1 - T_0} \right), \Omega = \frac{(T_1 - T_0)}{T_0}, \Gamma = \frac{RD_B F_0}{\mathcal{K}_f}, \Lambda = \frac{F_1 - F_0}{F_0}. \tag{21}$$

For a nanofluid, the viscosity model can be defined as [37]:

$$\mu_{nf} = \frac{\mu_f}{(1 - \bar{\phi})^{2.5}}, \tag{22}$$

where  $\mu_f$  the viscosity of base fluid, and  $\bar{\phi}$  is the solid volume fraction which is valid for  $0.01 \ll \bar{\phi} \ll 0.04$ . When the thermal conductivity of the particle is over 100 times larger than that of base fluid then the thermal conductivity in the sense of macroscopic effective medium theory known as the Maxwell model given as [37]:

$$\mathcal{K}_{nf} = \frac{\kappa_p + 2\kappa_f + 2\bar{\phi}(\kappa_p - \kappa_f)}{\kappa_p + 2\kappa_f - \bar{\phi}(\kappa_p - \kappa_f)} \kappa_f, \frac{\sigma_{nf}}{\sigma_f} = 1 + \frac{3(\bar{\gamma} - 1)\bar{\phi}}{(\bar{\gamma} + 2) - \bar{\gamma}(\bar{\gamma} - 1)\bar{\phi}}, \bar{\gamma} = \frac{\sigma_s}{\sigma_f}. \tag{23}$$

here,  $\kappa_p, \kappa_f$  are the thermal conductivities of the nano-particle and nanofluid;  $\sigma_s$  and  $\sigma_f$  are the electrical conductivity of the nano-particle and base fluid, respectively.

#### 4. Solution of the Problem

The solution of the above non-linear coupled partial differential equation can be solved with the help of the homotopy perturbation method (HPM). The homotopy for Equations (13)–(15) can be written as:

$$\mathcal{H}(w, \tilde{q}) = (1 - \tilde{q}) (L_1(w) - L_1(\bar{w}_0)) + \tilde{q} \left( L_1(w) + We \frac{\partial}{\partial y} \left( \frac{\partial w}{\partial y} \right)^2 + Gr_T \Theta - Gr_T \vartheta - \frac{\partial p}{\partial x} \right), \tag{24}$$

$$\mathcal{H}(\Theta, \tilde{q}) = (1 - \tilde{q}) (L_2(\Theta) - L_2(\bar{\Theta}_0)) + \tilde{q} \left( L_2(\Theta) + \frac{Pr}{1 + R_n Pr} \left( N_b \frac{\partial \vartheta}{\partial y} \frac{\partial \Theta}{\partial y} + N_t \left( \frac{\partial \vartheta}{\partial y} \right)^2 \right) + \frac{Pr\beta}{1 + R_n Pr} \right), \tag{25}$$

$$\mathcal{H}(\vartheta, \tilde{q}) = (1 - \tilde{q}) (L_2(\vartheta) - L_2(\bar{\vartheta}_0)) + \tilde{q} \left( L_2(\vartheta) + \frac{N_t}{N_b} \left( \frac{\partial^2 \Theta}{\partial y^2} \right) - \gamma \vartheta \right). \tag{26}$$

The linear operators  $L_1, L_2$  are taken in the following form:

$$L_1 = \frac{\partial^2}{\partial y^2} - M^2 - \frac{1}{k}, \tag{27}$$

$$L_2 = \frac{\partial^2}{\partial y^2}, \tag{28}$$

and the initial guess for the above linear operators are defined as:

$$\bar{w}_0 = \frac{\cosh N^2 y - \cosh N^2 h}{\cosh N^2 h}, \tag{29}$$

$$\bar{\vartheta}_0 = \bar{\Theta}_0 = \frac{y}{h}. \tag{30}$$

Defining the following expansion:

$$w(x, y) = w_0(x, y) + \tilde{q}w_1(x, y) + \tilde{q}^2w_2(x, y) + \dots, \tag{31}$$

$$\Theta(x, y) = \Theta_0(x, y) + \tilde{q}\Theta_1(x, y) + \tilde{q}^2\Theta_2(x, y) + \dots, \tag{32}$$

$$\vartheta(x, y) = \vartheta_0(x, y) + \tilde{q}\vartheta_1(x, y) + \tilde{q}^2\vartheta_2(x, y) + \dots, \tag{33}$$

Using Equations (31)–(33) in Equations (24)–(26), and comparing the powers of  $\tilde{q}$ , we get a system of linear differential equations with their relevant boundary conditions. According to scheme of HPM, we obtained the solution as  $\tilde{q} \rightarrow 1$ , we get:

$$u(x, y) = w(x, y) = w_0(x, y) + w_1(x, y) + w_2(x, y) + \dots, \tag{34}$$

$$\theta(x, y) = \Theta(x, y) = \Theta_0(x, y) + \Theta_1(x, y) + \Theta_2(x, y) + \dots, \tag{35}$$

$$\Phi(x, y) = \vartheta(x, y) = \vartheta_0(x, y) + \vartheta_1(x, y) + \vartheta_2(x, y) + \dots, \tag{36}$$

The solution of the velocity profile, temperature profile, and nano-particle concentration are written in simplified form as:

$$\begin{aligned} u = & \frac{\cosh N^2 y - \cosh N^2 h}{\cosh N^2 h} + \frac{1}{12h} \operatorname{sech}^2 hN^2 \left( -3h(h-y) \left( h \left( N^2 + \frac{dp}{dx} \right) + 2N^4 We + \right. \right. \\ & \left. \left( N^2 + \frac{dp}{dx} \right) y \right) + Gr_T (h^3 - y^3) + Gr_F (-h^3 + y^3) + \left( -h^3 \left( Gr_F - Gr_T + 3 \left( N^2 + \frac{dp}{dx} \right) \right) + \right. \\ & \left. 3h \left( N^2 + \frac{dp}{dx} \right) y^2 + (Gr_F - Gr_T) y^3 \right) \cosh 2hN^2 + 3hN^2 We (\sinh 2hN^2 - \sinh 2yN^2) \Big) + \\ & \frac{1}{1440h^2N^4(1+PrR_n)} \operatorname{sech}^3 hN^2 \left( 3 \left( 15Gr_T (h^4N^4(N_b + N_t)Pr + N^4(N_b + N_t)Pr y^4 - \right. \right. \\ & 2h(12(1 + PrR_n)We + N^4(N_b + N_t)Pr y^3) + h^6N^4Pr\beta + h^2N^4Pr y^4\beta - \\ & 2h^3N^4(6(1 + PrR_n)We + Pr y^3\beta)) + h(1 + PrR_n) \left( 360hN^4We \left( h \left( N^2 + \frac{dp}{dx} \right) + \right. \right. \\ & \left. \left. N^4We \right) + Gr_F(180(2 + h^2N^4)We + N^4(7h^5 - 10h^2y^3 + 3y^5)\gamma) \right) \Big) \cosh hN^2 + \\ & \left( 15Gr_T (h^4N^4(N_b + N_t)Pr + N^4(N_b + N_t)Pr y^4 - 2h(12(1 + PrR_n)We + \right. \\ & \left. N^4(N_b + N_t)Pr y^3) + h^6N^4Pr\beta + h^2N^4Pr y^4\beta - 2h^3N^4(6(1 + PrR_n)We + Pr y^3\beta)) + \right. \\ & \left. h(1 + PrR_n) \left( 120hN^4We \left( 3h \left( N^2 + \frac{dp}{dx} \right) - N^4We \right) + Gr_F(180(2 + h^2N^4)We + \right. \right. \\ & \left. \left. N^4(7h^5 - 10h^2y^3 + 3y^5)\gamma) \right) \right) \cosh 3hN^2 - 60h(1 + PrR_n)We(3(2hN^4(N^2 + \\ & dp/dx)y + Gr_F(2 + N^4y^2) - Gr_T(2 + N^4y^2)) \cosh N^2(2h - y) + 6(hN^4(3N^4We + \\ & 2N^2y + 2ydp/dx) + Gr_F(2 + N^4y^2) - Gr_T(2 + N^4y^2)) \cosh yN^2 - \\ & 2hN^8We \cosh 3yN^2 + 6Gr_F \cosh N^2(2h - y) - 6Gr_T \cosh N^2(2h - y) + \\ & 6hN^6y \cosh N^2(2h - y) + 6hN^4dp/dx y \cosh N^2(2h - y) + 3Gr_F N^4y^2 \cosh N^2(2h - \\ & y) - 3Gr_T N^4y^2 \cosh N^2(2h - y) + 6Gr_F hN^2 \sinh hN^2 - 6Gr_T hN^2 \sinh hN^2 + \\ & 6hN^4 \sinh hN^2 + 6hN^2 dp/dx \sinh hN^2 + 6Gr_F hN^2 \sinh 3hN^2 - 6Gr_T hN^2 \sinh 3hN^2 + \\ & 6hN^4 \sinh hN^2 + 6hN^2 dp/dx \sinh 3hN^2 + 6hN^4 \sinh N^2(2h - y) + 6hN^2 dp/ \\ & dx \sinh N^2(2h - y) + 6Gr_F N^2y \sinh N^2(2h - y) - 6Gr_T N^2y \sinh N^2(2h - y) - \\ & 12hN^4 \sinh N^2y - 12hN^2 dp/dx \sinh N^2y - 12Gr_F N^2y \sinh N^2y + \\ & 12Gr_T N^2y \sinh N^2y - 6hN^4 \sinh N^2(2h + y) - 6hN^2 dp/dx \sinh N^2(2h + y) - \\ & 6Gr_F N^2y \sinh N^2(2h + y) + 6Gr_T N^2y \sinh N^2(2h + y) \Big), \end{aligned} \tag{37}$$

$$\theta = \frac{y}{h} - \left( \frac{1}{24h^3(1 + \text{PrR}_n)^2} \right) (\text{Pr}(h - y)y(-2h(12N_t + N_b(6 + (N_b + N_t)\text{Pr}) + 6(N_b + 2N_t)\text{PrR}_n) + 4N_b(N_b + N_t)\text{Pr}y - 2h^3)(6 + N_b\text{Pr} + 6\text{PrR}_n)\beta + 4h^2N_b\text{Pr}y\beta + hN_b(1 + \text{PrR}_n)(h^2 - hy - y^2)\gamma), \quad (38)$$

$$\Phi = \frac{y}{h} + \left( \frac{-4h^2(h^2 - 3y^2)\gamma}{24h^3} \right) + \left( \frac{1}{24h^3N_b(1 + \text{PrR}_n)^2} \right) (y(-2N_t\text{Pr}(h - y)(h(N_b^2\text{Pr} + N_t(6 + N_b\text{Pr} + 6\text{PrR}_n)) - 2N_b(N_b + N_t)\text{Pr}y + h^3N_b\text{Pr}\beta - 2h^2N_b\text{Pr}y\beta) + hN_bN_t\text{Pr}(1 + \text{PrR}_n)(h^3 - 2h^2y + y^3)\gamma + h^2N_b(1 + \text{PrR}_n)^2(h^3 - 2h^2y + y^3)\gamma^2)), \quad (39)$$

where  $N^2 = M^2 + \frac{1}{k}$ .

The instantaneous volume rate is defined as:

$$Q = \int_0^h u dy. \quad (40)$$

The non-dimensional form of the pressure rise  $\Delta P_L$  and friction force  $\Delta F_L$  along the wall with a length of the non-uniform channel  $L$  is given by:

$$\Delta P_L = \int_0^{L/\lambda} \frac{dp}{dx} dx, \quad (41)$$

$$\Delta F_L = \int_0^{L/\lambda} h \left( -\frac{dp}{dx} \right) dx. \quad (42)$$

## 5. Numerical Results and Discussion

In this section influence of different parameters of interest are investigated graphically. To discuss the above results more vigorously, we assume that for instantaneous volume flow rate  $Q(x, t)$  is periodic in  $(x - t)$  and is defined by:

$$Q(x, t) = \bar{Q} + \phi \sin 2\pi(x - t),$$

where  $\bar{Q}$  describes the average time flow over one period of the wave. With the help of this form  $Q(x, t)$ , we will numerically compute the pressure rise ( $\Delta P_L$ ) and friction force ( $\Delta F_L$ ) over the length  $L$  of the non-uniform channel. A graphical demonstration for temperature profile, concentration distribution, pressure rise, friction force, and entropy generation are plotted for all of the physical parameters, such as Brownian motion ( $N_b$ ), Prandtl number ( $\text{Pr}$ ), thermophoresis parameter ( $N_t$ ), chemical reaction parameter ( $\gamma$ ), heat source/sink parameter ( $\beta$ ), Hartmann number ( $M$ ), porosity parameter ( $k$ ), Brinkman number ( $B_r$ ), dimensionless temperature difference ( $\Omega$ ), concentration difference ( $\Lambda$ ), constant parameter ( $\zeta$ ), and diffusive coefficient ( $\Gamma$ ).

From Figure 2 it can be observed that temperature profile is increasing throughout the domain with the increase in the parameters  $\beta$  and  $N_t$ . According to Equations (14) and (15), the thermophoresis parameter is directly proportional to the temperature profile; thus, with the increase in  $N_t$  temperature profile increases. Figure 3 shows that the temperature profile also increases when  $N_b$  and  $\text{Pr}$  increase. Brownian motion creates micro-mixing which raises the thermal conductivity while an increase in the  $\text{Pr}$  thinner thermal boundary layer forms. It can be observed from Figure 4a that, when the chemical parameter increases, the concentration profile shows opposite behavior near the walls of the channel. The concentration profile describes the same behavior for  $N_b$  and  $N_t$  in Figures 4b and 5a. Entropy generation is plotted in Figures 5b, 6 and 7 for different values of  $B_r$ ,  $\Gamma$ ,  $\Lambda$ ,  $\zeta$ , and  $\Omega$ . It has been investigated that the behavior of entropy generation is increasing with the increment in  $B_r$ ,  $\Gamma$ ,  $\Lambda$ ,  $\zeta$  and remains uniform throughout the domain. In Figure 7b we can observe that the behavior is opposite

when the parameter  $\Omega$  increases. The reason behind these behaviors of entropy generation is that the Brinkman parameter is directly proportional to the square of the velocity profile of the flow; hence, entropy generation increases with the increase in  $B_r$  while  $\Omega$  is inversely proportional to the velocity distribution which causes a decrease in entropy generation for larger values of  $\Omega$ . Additionally, it is important to note that  $\zeta$  is the ratio of the dimensionless concentration difference to the dimensionless temperature difference. The parameters  $\zeta$  and  $\Gamma$  indicate the contribution of mass transfer to the entropy generation. Figures 8, 9 and 10a are displayed to analyze the pressure rise corresponding to the variation of the numerical values of the different parameters  $Gr_T, Gr_F, k, M,$  and  $We$ . In Figure 8a, it is noticed that the pressure rise is decreasing with the increase in  $Gr_F$  while, in Figure 8b, it is concluded that its behavior is opposite for ( $Gr_T$ ). It can be analyzed from Figure 9a that the pressure rise increases when the porosity parameter ( $k$ ) increases. It can also be seen from Figure 9b that when the Hartmann number ( $M$ ) increases, then the pressure rise decreases. This phenomena describes the fact that a suitable magnetic field can be applied to control the pressure and the pressure decreasing means that the flow can pass easily without imposing higher pressure. It is concluded from Figure 9a that the pressure rise increases with the increase in the Weissenberg number ( $We$ ). The graphical results for friction forces are plotted in Figures 10b, 11 and 12. It can be observed from all of these figures that the friction forces show completely opposite behavior for all the physical parameters as compared to the pressure rise.

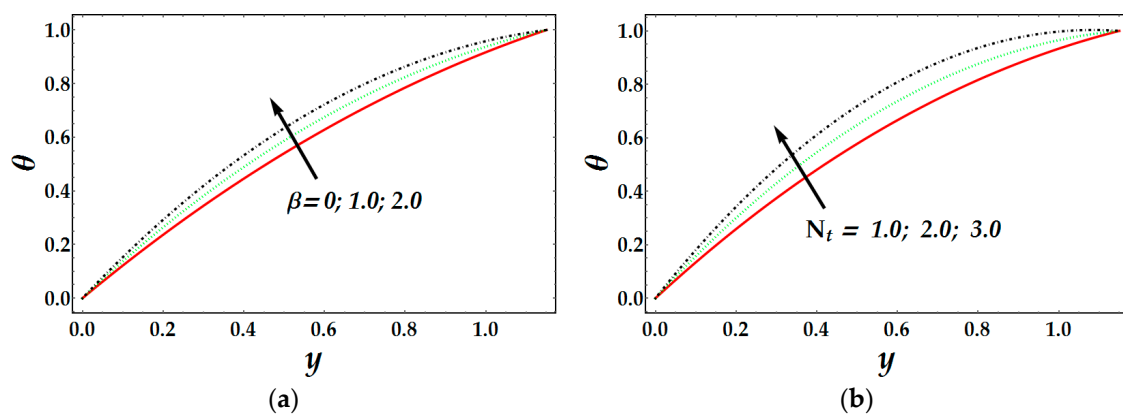


Figure 2. Temperature distribution for various values of  $\beta$  and  $N_t$  when  $N_b = 0.5, We = 0.2, M = 0.1, Gr_T = 0.5, Gr_F = 0.6, \gamma = 0.1, k = 1, Pr = 0.5$ .

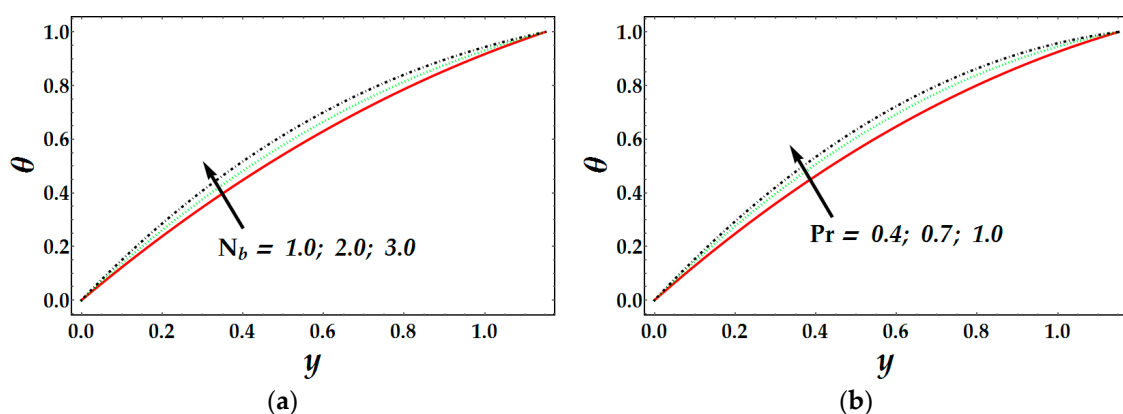


Figure 3. Temperature distribution for various values of  $Pr$  and  $N_b$  when  $N_t = 1, \beta = 0.8, We = 0.2, M = 0.1, Gr_T = 0.5, Gr_F = 0.6, \gamma = 0.1, k = 1$ .

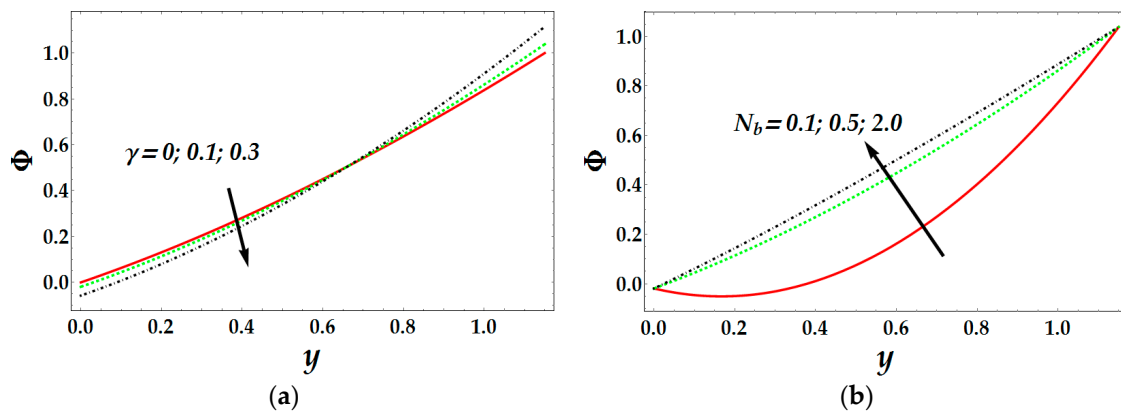


Figure 4. Concentration distribution for various values of  $N_b$  and  $\gamma$  when  $N_b = 0.5, \beta = 0.8, We = 0.2, M = 0.1, Gr_T = 0.5, Gr_F = 0.6, k = 1, Pr = 0.5$ .

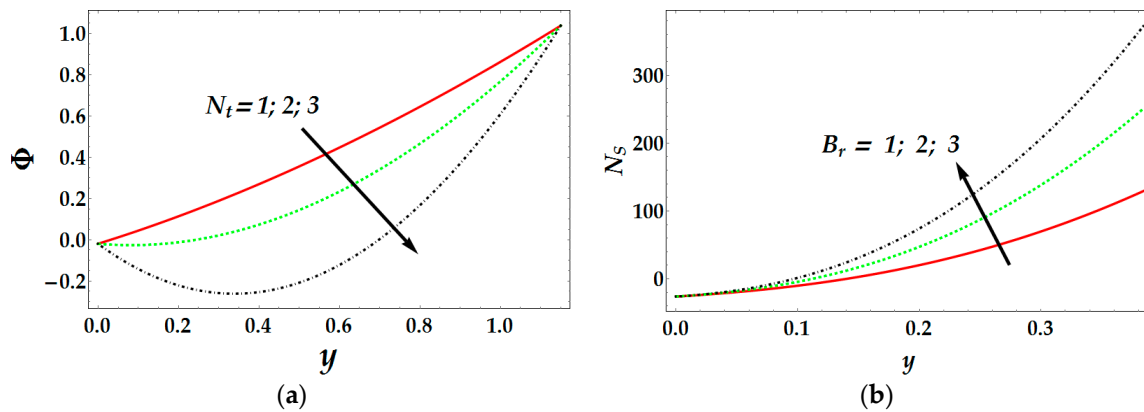


Figure 5. (a) Concentration distribution for various values of  $N_t$ ; and (b) entropy generation for various values of  $B_r$  when  $N_b = 0.5, \beta = 0.8, We = 0.2, M = 0.1, Gr_T = 0.5, Gr_F = 0.6, \gamma = 0.1, k = 1, Pr = 0.5$ .

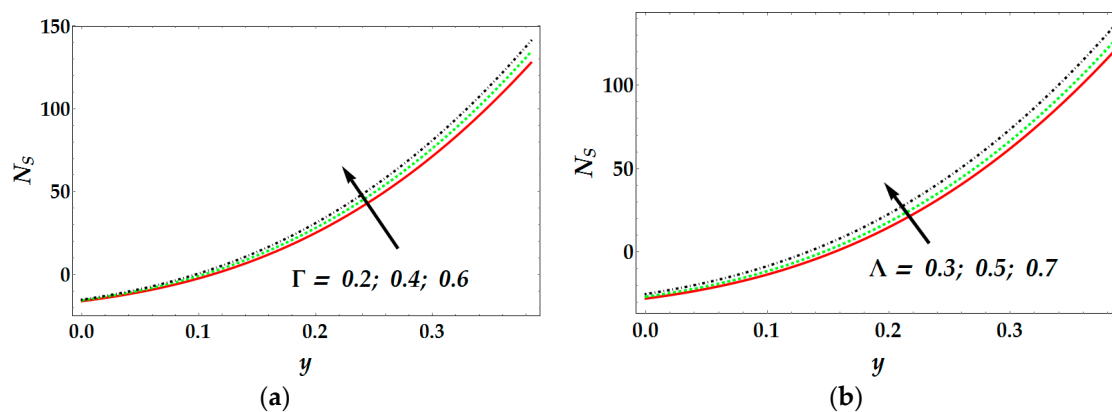
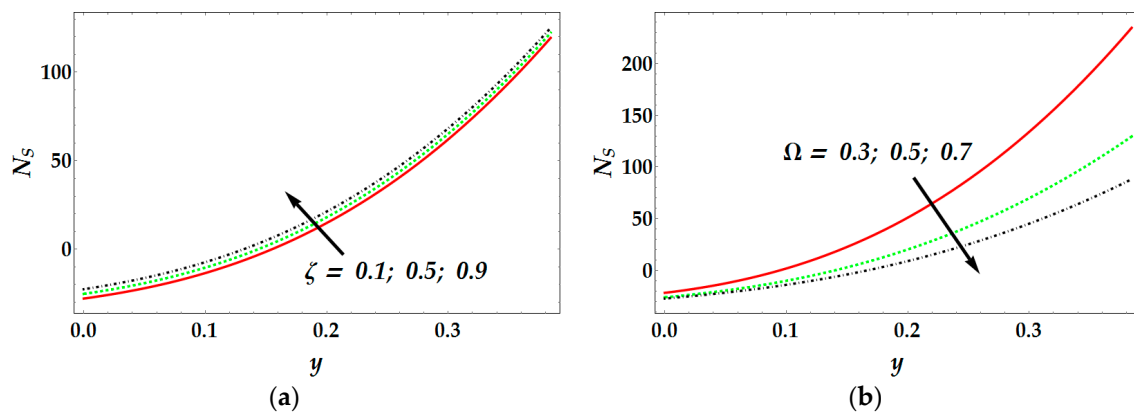
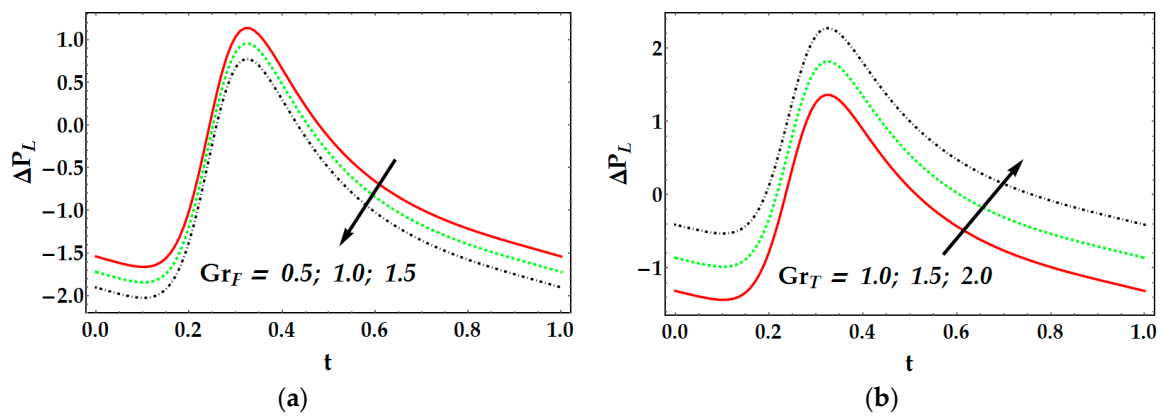


Figure 6. Entropy generation for various values of  $\Gamma$  and  $\Lambda$  when  $N_b = 0.5, N_t = 1, \beta = 0.8, We = 0.2, M = 0.1, Gr_T = 0.5, Gr_F = 0.6, \gamma = 1, k = 1, Pr = 0.5$ .



**Figure 7.** Entropy generation for various values of  $\zeta$  and  $\Omega$  when  $N_b = 0.5, N_t = 1, \beta = 0.8, We = 0.2, M = 0.1, Gr_T = 0.5, Gr_F = 0.6, \gamma = 1, k = 1, Pr = 0.5$ .



**Figure 8.** Pressure rise for various values of  $Gr_F$  and  $Gr_T$  when  $N_b = 0.5, N_t = 1, \beta = 0.8, We = 0.2, M = 0.1, \gamma = 0.1, k = 1, Pr = 0.5$ .

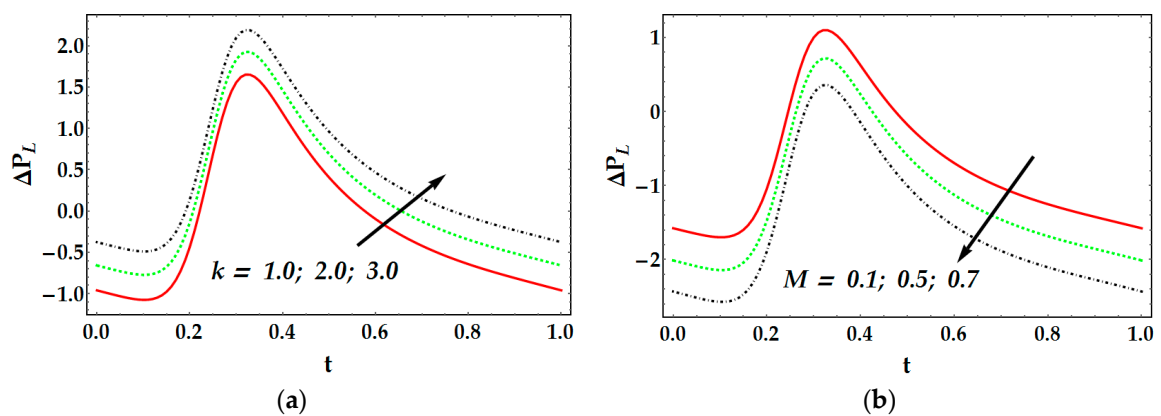


**Figure 9.** Pressure rise for various values of  $k$  and  $M$  when  $N_b = 0.5, N_t = 1, \beta = 0.8, We = 0.2, Gr_T = 0.5, Gr_F = 0.6, \gamma = 0.1, Pr = 0.5$ .

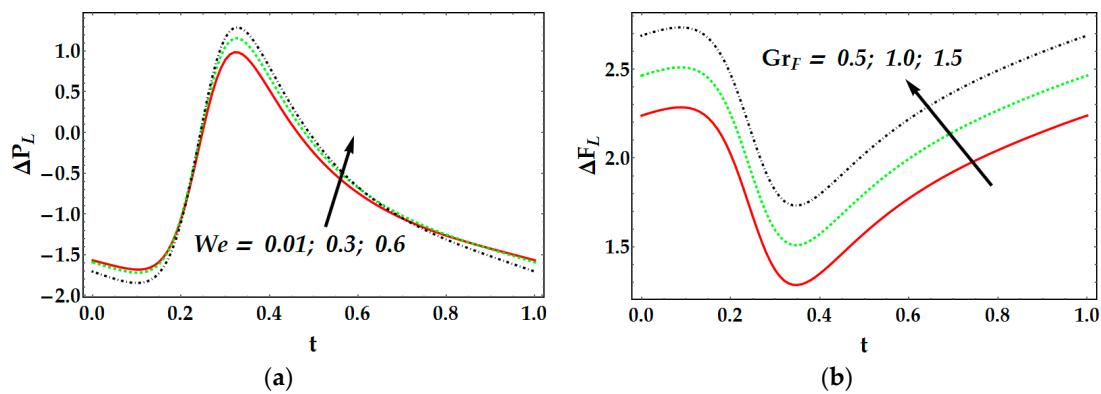


**Figure 10.** (a) Pressure rise for various values of  $We$ ; and (b) friction forces for various values of  $Gr_F$  when  $N_b = 0.5, N_t = 1, \beta = 0.8, M = 0.1, Gr_T = 0.5, \gamma = 0.1, k = 1, Pr = 0.5$ .

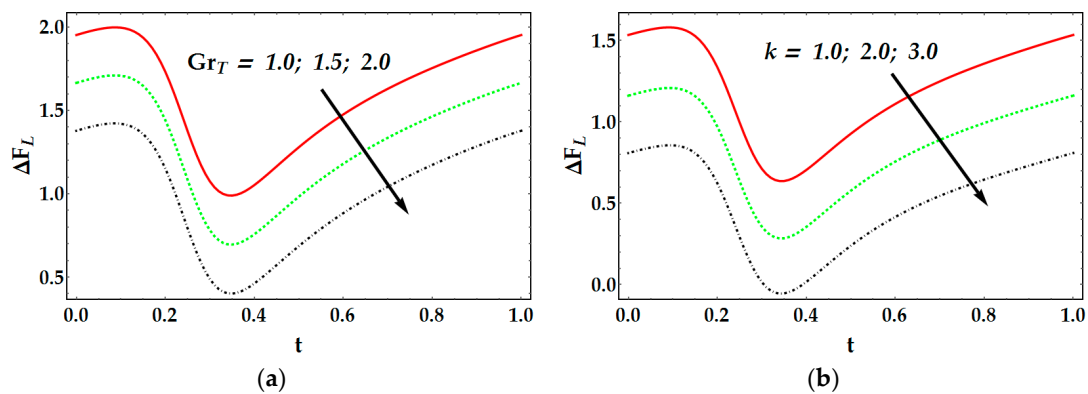


**Figure 11.** Friction forces for various values of  $Gr_T$  and  $k$  when  $N_b = 0.5, N_t = 1, \beta = 0.8, We = 0.2, M = 0.1, Gr_F = 0.6, \gamma = 0.1, Pr = 0.5$ .

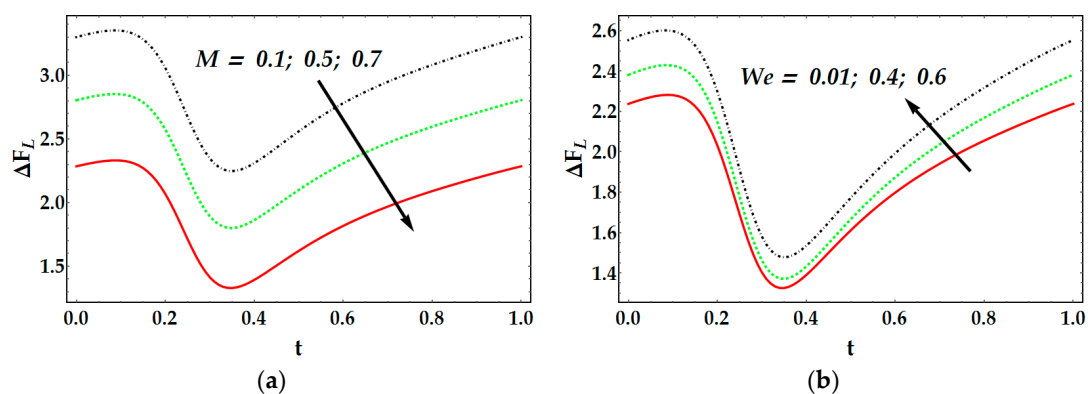


**Figure 12.** Friction forces for various values of  $M$  and  $We$  when  $N_b = 0.5, N_t = 1, \beta = 0.8, Gr_T = 0.5, Gr_F = 0.6, \gamma = 0.1, k = 1, Pr = 0.5$ .

Moreover, In Equation (13), by taking  $We = M = 0, k \rightarrow \infty, Gr_T = Gr_F = 0$ , the present results can be reduced to the results obtained by Shapiro *et al.* [39] and Srivastava and Srivastava [40] for a Newtonian fluid case (Power Law index  $n = 1$ ). Moreover, Equation (13) can also reduce to the same results obtained by Gupta and Seshadri [41] by taking  $We = 0, k \rightarrow \infty, Gr_T = Gr_F = 0$ . The present analysis can also be reduced to the similar results obtained by Mekheimer [42] for a Newtonian fluid (couple stress parameter  $\gamma \rightarrow \infty$ ) by taking  $We = 0, k \rightarrow \infty, Gr_T = Gr_F = 0$ . The graphical results are shown in Figure 13.

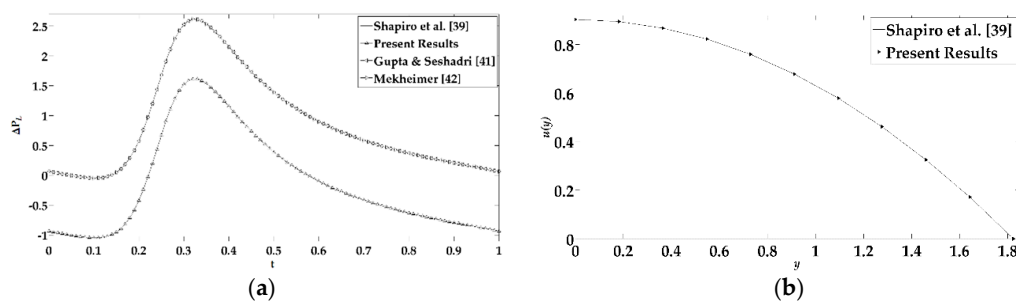


Figure 13. (a) Comparison of pressure rise; (b) Comparison of velocity profile.

## 6. Conclusions

In this article, entropy generation on MHD blood flow of a nanofluid induced by a sinusoidal wave has been investigated. The governing equation for the blood flow problem is modeled with the help of continuity, momentum, and nano-particle equations. The resulting nonlinear coupled partial differential equation has been solved with the help of the homotopy perturbation method (HPM). The expressions for pressure rise and friction forces are calculated numerically with the help of computational software Mathematica (10.3v). The major outcomes for the present analysis are:

- The temperature profile increases with the increase in  $N_t$  and  $N_b$ , while friction force reduces with the increment of these parameters.
- The concentration distribution for chemical reactions parameter is opposite near the walls.
- The temperature profile and velocity profile play vital roles to measure entropy generation by increases in  $B_r$ ,  $\Omega$ ,  $\Lambda$ ,  $\varepsilon$ , and  $\Gamma$ .
- The pressure rise increases with the increase in density Grashof number and thermal Grashof number, but its behavior is opposite for friction forces, which indicates the fact that with the increase in these parameters, pressure rise can be controlled and can also enhance peristaltic pumping performance.
- The pressure rise also increases for nanofluid thermal conductivity, Weissenberg number, and Hartmann number, but friction force behavior for these parameters are totally different. It provides a great importance at the time of surgery and critical operations to control excessive bleeding.
- The present analysis can also be reduced to a Newtonian nanofluid by taking  $We = 0$  as a special case for our study.

**Acknowledgments:** The authors extend their appreciation to the Deanship of Scientific Research at King Saud University for funding this work through the research group project No RGP-VPP-080.

**Author Contributions:** Mohammad Mehdi Rashidi and Munawwar Ali Abbas conceived and designed the mathematical formulation of the problem, whereas solution of the problem and graphical results are analyzed by Mohamed El-Sayed Ali and Muhammad Mubashir Bhatti.

**Conflicts of Interest:** The authors declare no conflict of interest.

## Nomenclature

$\tilde{u}, \tilde{v}$	velocity components (m/s)
$\tilde{x}, \tilde{y}$	Cartesian coordinate (m)
$\tilde{p}$	pressure in fixed frame ( $\text{N/m}^2$ )
$\tilde{a}$	wave amplitude (m)
$b(\tilde{x})$	width of the channel (m)
$\tilde{c}$	wave velocity (m/s)
Pr	Prandtl number
Re	Reynolds number

$\tilde{t}$	time (s)
$Gr_F$	basic density Grashof number
$Gr_T$	thermal Grashof number
$N_b$	Brownian motion parameter
$N_t$	thermophoresis parameter
$\bar{K} (\ll 1)$	constant
$A_1$	Rivlin Erickson tensor
$B_0$	magnetic field (T)
$We$	Weissenberg number
$R_n$	radiation parameter
$Q$	volume flow rate ( $m^3/s$ )
$T, F$	temperature (K) and concentration
$T_0, T_1$	Temperature at centre and at the wall
$F_0, F_1$	Nanoparticle fraction at centre and at the wall
$B_r$	Brinkman number
$\tilde{q}$	Perturbation parameter
$g$	acceleration due to gravity ( $m/s^2$ )
$D_B$	Brownian diffusion coefficient ( $m^2/s$ )
$D_T$	thermophoretic diffusion coefficient ( $m^2/s$ )
$K$	mean absorption constant
$M$	Hartman number
$S$	stress tensor
$\tilde{k}$	porosity parameter

### Greek Symbols

$\gamma$	chemical reaction parameter
$\kappa$	nanofluid thermal conductivity (W/m K)
$\beta$	heat source/sink parameter
$\mu$	viscosity of the fluid ( $N s/m^2$ )
$\Phi$	nano-particle volume fraction
$\sigma$	electrical conductivity (S/m)
$\Omega$	dimensionless temperature difference
$\Lambda$	concentration difference
$\zeta$	constant parameter
$\Gamma$	diffusive coefficient
$\dot{\gamma}$	Second invariant tensor
$\delta$	wave number ( $m^{-1}$ )
$\bar{\sigma}$	Stefan Boltzmann constant
$c_p$	effective heat capacity of nanoparticle (J/K)
$\nu$	nanofluid kinematic viscosity ( $m^2/s$ )
$(\rho)_p$	nanoparticle mass density ( $kg/m^3$ )
$\rho_f$	fluid density ( $kg/m^3$ )
$\rho_{f_0}$	fluid density at the reference temperature ( $T_0$ ) ( $kg/m^3$ )
$\zeta$	volumetric expansion coefficient of the fluid
$(\rho c)_f$	heat capacity of fluid (J/K)
$\lambda$	wavelength (m)
$\phi$	Amplitude ratio

## References

1. Choi, S.U.S. Enhancing thermal conductivity of fluids with nanoparticles. *ASME Int. Mech. Eng. Congr. Expos.* **1995**, *231*, 99–106.
2. Huminic, G.; Huminic, A. Heat transfer characteristics in double tube helical heat exchangers using Nanofluids. *Int. J. Heat Mass. Trans.* **2011**, *54*, 4280–4287. [[CrossRef](#)]
3. Duangthongsuk, W.; Wongwises, S. Heat transfer enhancement and pressure drop characteristics of TiO<sub>2</sub>-water nanofluid in a double-tube counter flow heat exchanger. *Int. J. Heat Mass. Trans.* **2009**, *52*, 2059–2067. [[CrossRef](#)]
4. Li, J.; Kleinstreuer, C. Thermal performance of nanofluid flow in microchannels. *Int. J. Numer. Method Heat* **2008**, *29*, 1221–1232. [[CrossRef](#)]
5. Duangthongsuk, W.; Selim Dalkilic, A.; Wongwises, S. Convective heat transfer of Al<sub>2</sub>O<sub>3</sub>-water nanofluids in a microchannel heat sink. *Curr. Nanosci.* **2012**, *8*, 317–322. [[CrossRef](#)]
6. Li, J.; Kleinstreuer, C. Microfluidics analysis of nanoparticle mixing in a microchannel system. *Microfluid. Nanofluid.* **2009**, *6*, 661–668. [[CrossRef](#)]
7. Leong, K.Y.; Saidur, R.; Kazi, S.; Mamun, A.H. Performance investigation of an automotive car radiator operated with nanofluid-based coolants (nanofluid as a coolant in a radiator). *Appl. Therm. Eng.* **2010**, *30*, 2685–2692. [[CrossRef](#)]
8. Ali, M.; El-leathy, A.; Al-Sofyany, Z. The effect of nanofluid concentration on the cooling system of a vehicles radiator. *Adv. Mech. Eng.* **2014**. [[CrossRef](#)]
9. Rashidi, M.M.; Keimanesh, M.; Rajvanshi, S.C. Study of pulsatile flow in a porous annulus with the homotopy analysis method. *Int. J. Numer. Method Heat* **2012**, *22*, 971–989. [[CrossRef](#)]
10. Abbas, M.A.; Bai, Y.Q.; Bhatti, M.M.; Rashidi, M.M. Three dimensional peristaltic flow of hyperbolic tangent fluid in non-uniform channel having flexible walls. *Alex. Eng. J.* **2015**. [[CrossRef](#)]
11. Cosmi, F.; Di Marino, F. Modelling of the mechanical behaviour of porous materials: A new approach. *Acta Bioeng. Biomech.* **2001**, *3*, 55–66.
12. Bég, O.A.; Keimanesh, M.; Rashidi, M.M.; Davoodi, M.; Branch, S.T. Multi-Step dtm simulation of magneto-peristaltic flow of a conducting Williamson viscoelastic fluid. *Int. J. Appl. Math. Mech.* **2013**, *9*, 1–24.
13. Majchrzak, E.; Dziatkiewicz, G.; Paruch, M. The modelling of heating a tissue subjected to external electromagnetic field. *Acta Bioeng. Biomech.* **2008**, *10*, 29–37. [[PubMed](#)]
14. Nicoll, P.A. The anatomy and behavior of the vascular systems in *Nereis virens* and *Nereis limbata*. *Biol. Bull.* **1954**, *106*, 69–82. [[CrossRef](#)]
15. Blair, G.S. An equation for the flow of blood, plasma and serum through glass capillaries. *Nature* **1959**, *183*, 613–614. [[CrossRef](#)] [[PubMed](#)]
16. Misra, J.C.; Sinha, A.; Shit, G.C. Theoretical analysis of blood flow through an arterial segment having multiple stenosis. *J. Mech. Med. Biol.* **2008**, *8*, 265–279. [[CrossRef](#)]
17. Ibsen, S.; Sonnenberg, A.; Schutt, C.; Mukthavaram, R.; Yeh, Y.; Ortac, I.; Heller, M.J. Recovery of Drug Delivery Nanoparticles from Human Plasma Using an Electrokinetic Platform Technology. *Small* **2015**, *11*, 5088–5096. [[CrossRef](#)] [[PubMed](#)]
18. Akbar, N.S.; Nadeem, S. Simulation of heat and chemical reactions on Reiner Rivlin fluid model for blood flow through a tapered artery with a stenosis. *Heat Mass Transf.* **2010**, *46*, 531–539. [[CrossRef](#)]
19. Bugliarello, G.; Sevilla, J. Velocity distribution and other characteristics of steady and pulsatile blood flow in fine glass tubes. *Biorheology* **1970**, *7*, 85–107. [[PubMed](#)]
20. Misra, J.C.; Pandey, S.K. Peristaltic transport of blood in small vessels: Study of a mathematical model. *Comput. Math. Appl.* **2002**, *43*, 1183–1193. [[CrossRef](#)]
21. Rashidi, M.M.; Keimanesh, M.; Bég, O.A.; Hung, T.K. Magnetohydrodynamic biorheological transport phenomena in a porous medium: A simulation of magnetic blood flow control and filtration. *Int. J. Numer. Method Biomed. Eng.* **2011**, *27*, 805–821. [[CrossRef](#)]
22. Abbas, M.A.; Bai, Y.Q.; Rashidi, M.M.; Bhatti, M.M. Application of drug delivery in Magnetohydrodynamics peristaltic blood flow of nanofluid in a non-uniform channel. *J. Mech. Med. Biol.* **2015**, *16*, 1650052. [[CrossRef](#)]
23. Wada, S.; Karino, T. Computational studies on LDL transfers from flowing blood to arterial walls. In *Clinical Application of Computational Mechanics to the Cardiovascular System*; Springer: Tokyo, Japan, 2000; pp. 157–173.
24. Agarwal, H.L.; Anwaruddin, B. Peristaltic flow of blood in a branch. *Ranchi Univ. Math. J.* **1984**, *15*, 111–121.

25. Sud, V.K.; Sekhon, G.S.; Mishra, R.K. Pumping action on blood by a magnetic field. *Bull. Math. Biol.* **1977**, *39*, 385–390. [[CrossRef](#)] [[PubMed](#)]
26. Abbasi, F.M.; Hayat, T.; Alsaedi, A.; Ahmed, B. Soret and Dufour effects on peristaltic transport of MHD fluid with variable viscosity. *Appl. Math. Inf. Sci.* **2014**, *8*, 211–219. [[CrossRef](#)]
27. Rashidi, M.M.; Freidoonimehr, N.; Momoniat, E.; Rostami, B. Study of nonlinear MHD tribological squeeze film at generalized magnetic Reynolds numbers using DTM. *PLoS ONE* **2015**, *10*, e0135004. [[CrossRef](#)] [[PubMed](#)]
28. Makinde, O.D.; Eegunjobi, A.S.; Tshela, M.S. Thermodynamics Analysis of Variable Viscosity Hydromagnetic Couette Flow in a Rotating System with Hall Effects. *Entropy* **2015**, *17*, 7811–7826. [[CrossRef](#)]
29. Sheikholeslami, M.; Rashidi, M.M.; Ganji, D.D. Numerical investigation of magnetic nanofluid forced convective heat transfer in existence of variable magnetic field using two phase model. *J. Mol. Liq.* **2015**, *212*, 117–126. [[CrossRef](#)]
30. Sonnino, G.; Evslin, J.; Sonnino, A. Minimum Dissipation Principle in Nonlinear Transport. *Entropy* **2015**, *17*, 7567–7583. [[CrossRef](#)]
31. Bejan, A. Second law analysis in heat transfer. *Energy* **1980**, *5*, 720–732. [[CrossRef](#)]
32. Bejan, A. *Entropy Generation Minimization: The Method of Thermodynamic Optimization of Finite-Size Systems and Finite-Time Processes*; CRC Press: Boca Raton, FL, USA, 1995.
33. Revellin, R.; Lips, S.; Khandekar, S.; Bonjour, J. Local entropy generation for saturated two-phase flow. *Energy* **2009**, *34*, 1113–1121. [[CrossRef](#)]
34. Salas, H.; Cuevas, S.; de Haro, M.L. Entropy generation analysis of magnetohydrodynamics induction devices. *J. Phys. D Appl. Phys.* **1999**, *32*. [[CrossRef](#)]
35. Ibáñez, G.; Cuevas, S.; de Haro, M.L. Optimization analysis of an alternate Magnetohydrodynamics generator. *Energy Convers. Manag.* **2002**, *43*, 1757–1771. [[CrossRef](#)]
36. Lee, M.Y.; Kim, H.J. Heat Transfer Characteristics of a Speaker Using Nano-Sized Ferrofluid. *Entropy* **2014**, *16*, 5891–5900. [[CrossRef](#)]
37. Rashidi, M.M.; Bagheri, S.; Momoniat, E.; Freidoonimehr, N. Entropy analysis of convective MHD flow of third grade non-Newtonian fluid over a stretching sheet. *Ain Shams Eng. J.* **2015**. [[CrossRef](#)]
38. Mahian, O.; Kianifar, A.; Kleinstreuer, C.; Moh'd, A.; Pop, I.; Sahin, A.Z.; Wongwises, S. A review of entropy generation in Nanofluid flow. *Int. J. Heat Mass Transf.* **2013**, *65*, 514–532. [[CrossRef](#)]
39. Shapiro, A.H.; Jaffrin, M.Y.; Weinberg, S.L. Peristaltic pumping with long wavelength at low Reynolds number. *J. Fluid Mech.* **1969**, *37*, 799–825. [[CrossRef](#)]
40. Srivastava, L.M.; Srivastava, V.P. Peristaltic transport of a power-law fluid: Application to the ductus efferentes of the reproductive tract. *Rheol Acta* **1988**, *27*, 428–433. [[CrossRef](#)]
41. Gupta, B.B.; Seshadri, V. Peristaltic pumping in non-uniform tubes. *J. Biomech.* **1976**, *9*, 105–109. [[CrossRef](#)]
42. Mekheimer, K.S. Peristaltic flow of blood under effect of a magnetic field in a non-uniform channels. *Appl. Math. Comput.* **2004**, *153*, 763–777. [[CrossRef](#)]



© 2016 by the authors; licensee MDPI, Basel, Switzerland. This article is an open access article distributed under the terms and conditions of the Creative Commons by Attribution (CC-BY) license (<http://creativecommons.org/licenses/by/4.0/>).